EEHG Seeding for LCLS-II

LCLS-II TN-14-14

11/18/2014

Gregg Penn

EEHG seeding for LCLS-II

G. Penn
Lawrence Berkeley National Laboratory

October 23, 2014
DRAFT

1 Introduction

In addition to using the self-amplified spontaneous emission (SASE) [1] and self-seeding [2, 3] schemes, LCLS-II [4] may also incorporate seeding using external lasers as a future additional capability. External seeding can improve stability in the timing and pulse energy, give more control over the pulse duration, and may lead to more coherent pulses. This note will explore the possibility of using echo-enabled harmonic generation (EEHG) [5] for producing coherent radiation at up to ~ 1 keV photon energy starting from conventional laser sources. An additional option is considered where the EEHG stage yields bunching at lower photon energies which is then upshifted through harmonic generation (but without using the "fresh-bunch" approach [6]). This second stage of harmonic generation will take the form of simply switching the undulator parameter to be resonant with a harmonic to take advantage of nonlinear harmonic bunching already present in the beam. No additional chicane should be required, although one could consider adding a chicane for more flexibility. EEHG has been demonstrated at NLCTA [7] up to the 15th harmonic (160 nm).

2 Beam parameters

The simulations shown below use particles obtained from start-to-end (S2E) simulations of the linac. The nominal parameters for the electron beam and the main undulator sections for producing radiation are given in Table 1. Local parameters will vary with position along the bunch. The electron bunch has a nominal current of 1 kA. Two bunch types from two different injector and linac settings are considered, with 100 pC and 300 pC of charge respectively. The longitudinal phase spaces of these beams are shown in Fig. 1. The slice emittance in the core of the beam is 0.30 micron for the 100 pC bunch and 0.43 micron for the 300 pC bunch, while the horizontal projected emittances are 1.1 micron and 2.3 micron. The current and energy spread profiles are shown in Fig. 2. Note that the energy spread depends on the settings of the laser heater and may be subject to significant changes. The emittance profiles are shown in Fig. 3.

Table 1: Beam and undulator parameters for soft x-ray production at LCLS-II.

Parameter	Symbol	Value
Electron Beam:		
Bunch charge	Q	100 – 300 pC
Electron energy	E	4 GeV
Peak current	I	1 kA
Emittance	ϵ_N	0.30 – 0.43 micron
Energy spread	σ_E	0.5 MeV
Beta function	β	15 m
Final undulators:		
Undulator period	λ_u	39 mm
Undulator segment length	$L_{\rm seg}$	3.4 m
Break length	L_b	1.2 m
Minimum magnetic gap	$g_{\rm min}$	7.2 mm
Maximum undulator parameter	$K_{\rm max}$	5.48
Maximum resonant wavelength	$\lambda_{\rm res}$	5.1 nm

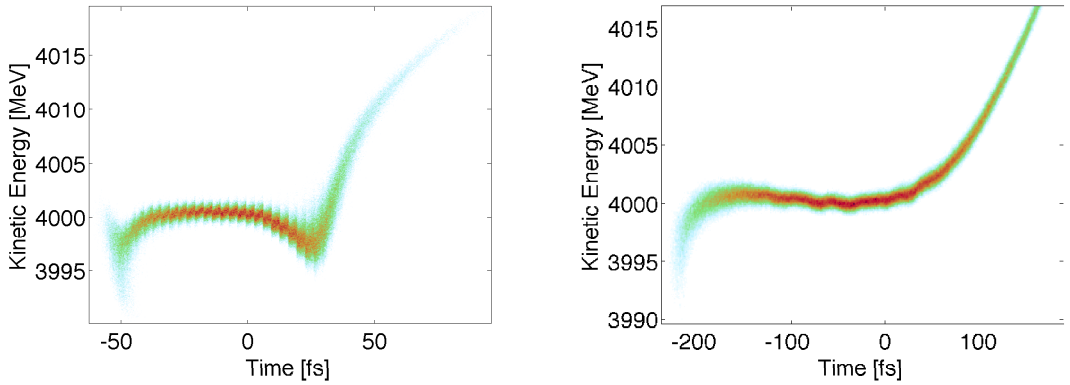

Figure 1: Longitudinal phase space density plots for the electron bunch at the entrance to the undulator hall, based on S2E studies. The bunch charge is 100 pC (left) and 300 pC (right).

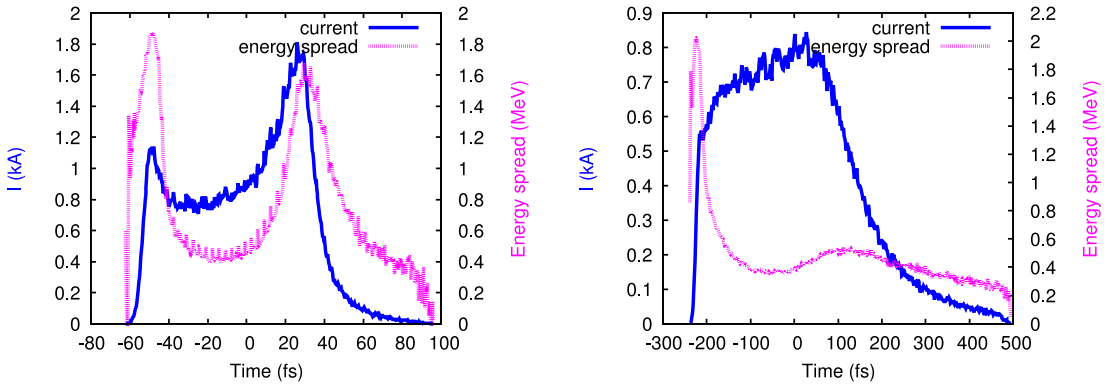

Figure 2: Current and energy spread profiles for the 100 pC bunch (left) and 300 pC bunch (right).

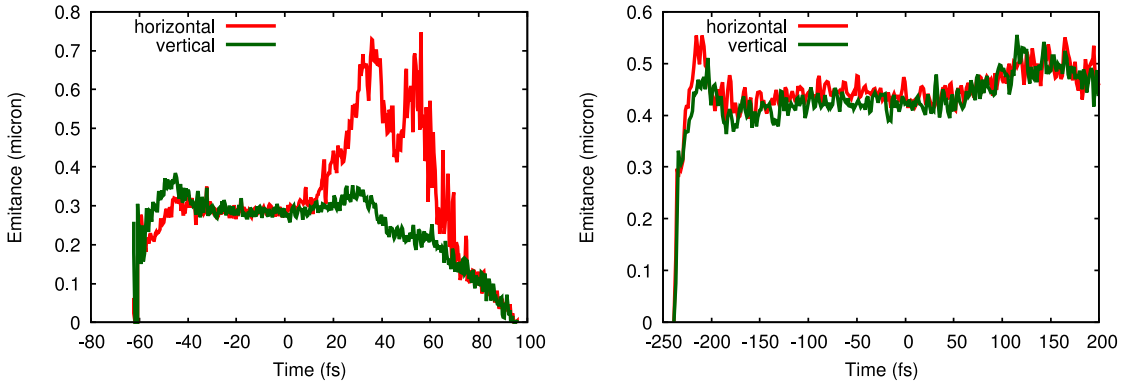

Figure 3: Emittance profiles for the 100 pC bunch (left) and 300 pC bunch (right).

The layout is shown in Fig. 4. The total number of undulators in the final stage may vary. Some of those undulators may be tuned to radiate at a harmonic of the wavelength produced through EEHG. FEL simulations were performed using GENESIS [8].

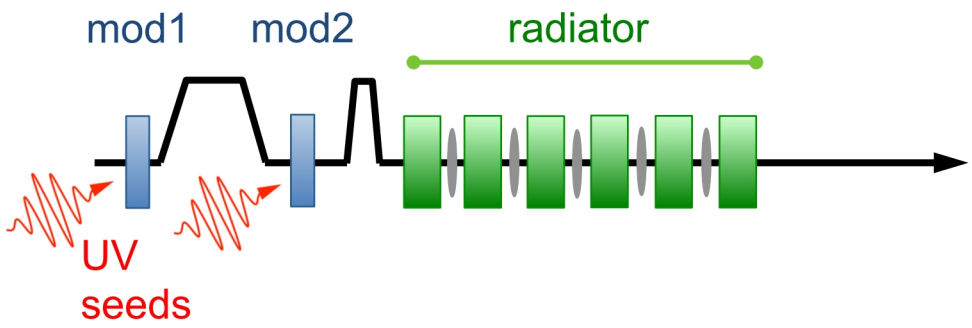

Figure 4: Beamline layout using EEHG, designed for wavelengths as short as 1 nm.

3 Echo design

Echo-enabled harmonic generation (EEHG) operates through a form of wave-mixing, where two energy modulations are used instead of one for standard HGHG. The first modulation is followed by a chicane which severely overbunches the modulation, creating well-separated bands in longitudinal phase space. Each band has a reduced energy spread. The second modulation is also followed by a chicane but in this case they are tuned so as to perform a standard phase rotation of each band. The overall bunching factor can be significant even at very high harmonics.

We consider two seed lasers both with a wavelength of 260 nm. The first undulator is 3.2 m long, with a period of 0.1 m. The laser pulse going into this undulator has a nominal peak power of 47 MW, and generates an energy modulation of 1.5 MeV. This is followed by a chicane with 2-m long dipole magnets and small 0.25-m breaks to simultaneous minimize both the strength of the magnetic fields and the overall length of the chicane. The second undulator is also 3.2 m long but with a period of 0.4 m. The laser pulse going into this undulator has a peak power ranging up to 900 MW (3 MeV of energy modulation) to yield bunching at 1 nm. Both lasers have a Rayleigh length of 1 m, and a nominal FWHM duration of 100 fs. Variations in the pulse duration will be explored below. This is followed by a second, more compact chicane with 0.25-m long dipoles. The undulators following the chicane all have a 39-mm period. The undulators closest to the second chicane will radiate at the bunching wavelength produced through EEHG. Later undulators may be tuned to a harmonic of this wavelength.

The reason for the difference in undulator periods for the two modulating undulators is that in the second undulator the phase space bands in the beam are particularly sensitive

to energy scattering. Increasing the period lowers the magnetic field and reduces incoherent synchrotron radiation (ISR). For the same reason, the large dispersion required for the first chicane is obtained by increasing the length of the magnets rather than increasing the magnetic field. Thus, the first chicane is 9 m long while the second chicane is only 2 m long. Even without magnetic fields, there is intra-beam scattering (IBS) which pushes the design towards being as short as possible. The combined effect of both ISR and IBS reduces the bunching factor at 1 nm from an ideal value of 5.2% to roughly 1.4%. Due to the scaling of these two effects, parameters are chosen such that IBS has a slightly larger impact on bunching. The degradation in bunching from the first chicane is comparable to that in the second undulator, while there is much less of an impact within the second chicane. Because of the severity of the impact of scattering, the beamline is kept as compact as possible by not using any quadrupoles or additional breaks until after the first radiating undulator.

Without taking into effect the impact of scattering, the optimal bunching parameter would be given by the magnitude of

$$\begin{aligned}\hat{b} \;=\; & \sum_{m,p \;|\; k_X = k_2 p - k_1 m} \mathrm{e}^{\mathrm{i}(p\psi_2 - m\psi_1)}(-1)^p \\ & \times\; J_p(C_2\eta_{m2}) J_m(C_1\eta_{m1}) \int \mathrm{d}\eta f_\eta(\eta)\mathrm{e}^{-\mathrm{i}C_1\eta}\,, \end{aligned} \tag{1}$$

where $C_1 = k_X R_2 - k_1 m R_1$, $C_2 = k_X R_2$, $\psi_{1,2}$ are the laser phases, $k_{1,2}$ are the laser wavenumbers, and k_X is the target output wavenumber. The height of the two energy modulations are η_{m1} and η_{m2}, and $f_\eta(\eta)$ is the energy distribution function. For an initial Gaussian energy distribution centered at $\bar{\eta}$ with energy spread σ_η,

$$\int \mathrm{d}\eta f_\eta(\eta)\mathrm{e}^{-\mathrm{i}C_1\eta} = \mathrm{e}^{-iC_1\bar{\eta}}\mathrm{e}^{-C_1^2\sigma_\eta^2/2}\,. \tag{2}$$

Usually only one term in the summation contributes significantly to the bunching, and this term is generally selected to correspond to $m = 1$. In simulations, ISR is modelled according to the local dipole field in both undulators and the chicanes. IBS is treated as an additional energy scatter applied randomly to all macroparticles at a rate of roughly $(5.2\text{ keV})^2/\text{m}$. The scattering rate should vary based on the transverse co-ordinates of each electron, but is instead approximated as being the same for all electrons. Because the GENESIS does not include a model for IBS, the chicanes are simulated in a separate code [9]. To account for the scattering due to IBS which occurs within the second undulator, between the two chicanes, an extra random energy kick of about 9 keV is applied after the second energy modulation. IBS is neglected in other parts of the beamline because after the second chicane, the bunching is already formed and energy scattering should not have a large impact.

For the direct scheme producing bunching at 1 nm, the chicane strengths are ~ 14.9 mm and 56 μm respectively. Up to 12 undulator sections are needed after the second chicane to reach about 1 GW of peak power. Alternatively, we consider producing bunching at 2 nm. In this case, the second energy modulation can be reduced to 2 MeV, requiring 400 MW of peak power. The chicane strengths are 11.4 mm and 86 micron, respectively. The

bunching produced at 2 nm is 3.1%, down from a theoretical 6.5% without scattering. There is negligible bunching at 1 nm. It is still possible to upshift further to 1 nm by retuning some of the final undulators. Even without using a chicane, there will be significant bunching at 1 nm through nonlinear harmonic generation as the beam approaches saturation at 2 nm. However, because of the large energy spread the bunching typically does not grow any further after switching to a fundamental wavelength of 1 nm. This method [10] is a straightforward way to jump to a low harmonic. The EEHG stage could also yield bunching at 3 nm and then be upshifted by a further factor of 3, but for higher harmonics the required energy spread becomes quite large and the power produced drops significantly.

As a third option, we could produce bunching at 2 nm but also generate a significant amount of bunching at 1 nm as well straight from the EEHG stage. Then it is possible to go back and forth between initially radiating at 2 nm and jumping to 1 nm if desired, or just radiating directly at 1 nm using the bunching already produced. The latter case is equivalent to choosing $m = 2$. To accomplish this, the second energy modulation must again be increased to 3 MeV. The chicanes used have an R_{56} of 7.5 mm and 56 micron. The bunching produced at 2 nm is 4.9%, and the bunching at 1 nm is 1.0%; the bunching at 1 nm would be 3.3% without scattering. The bunching at 1 nm is smaller than the original example, because there is a penalty in the bunching produced using a configuration where $m = 2$ that more than offsets the benefit to using a weaker first chicane.

4 Simulation Results

We first compare results for the 100 pC bunch using two, 100-fs lasers as a seed, with that for the 300 pC bunch using two, 200-fs lasers. The increased bunch length of the 300 pC bunch allows for a more substantial benefit to using a longer pulse duration. The evolution of the pulse energy is shown in Fig. 5.

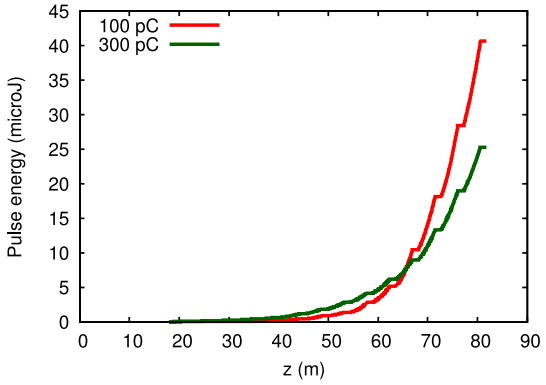

Figure 5: Evolution of the pulse energy at 1 nm produced directly through EEHG. Zero marks the start of the first modulating undulator.

The bunching at 1 nm at the start of the radiating undulators, and the final power profile at the end are shown in Fig. 6. Note that the 300 pC bunch has a smaller energy spread in

the core compared to that of the 100 pC bunch. This is why the initial bunching is larger for the 300 pC bunch even though the peak laser power of the laser seeds are unchanged. The output spectra are shown in Fig. 7. For the 300 pC case, the final pulse has a FWHM pulse duration of 45 fs fwhm and is nearly transform limited, with a fwhm bandwidth of 0.07 eV. For both the 100 pC and 300 pC bunches, the ratio of the duration of the output pulse to that of the second seed laser is roughly $1.4(\lambda_2/\lambda_X)^{1/3}$.

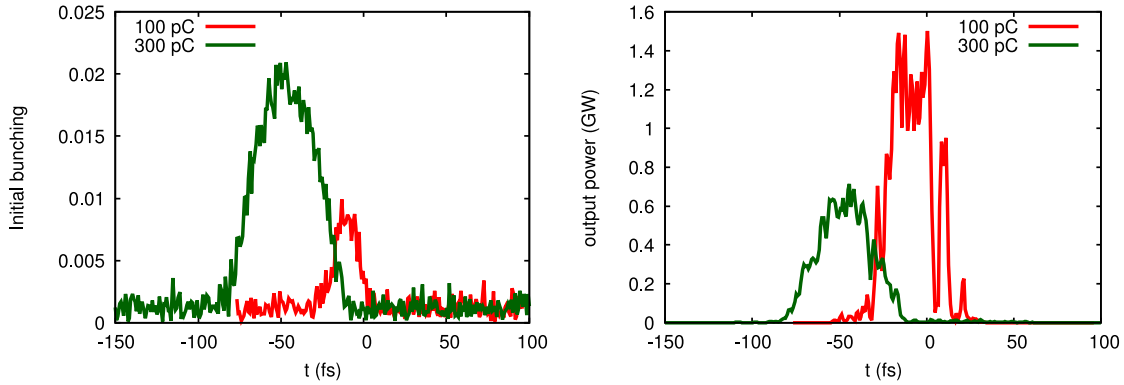

Figure 6: Initial bunching generated at 1 nm at $z = 17.9$ m (left) and output power profiles at 1 nm after 80 m (right).

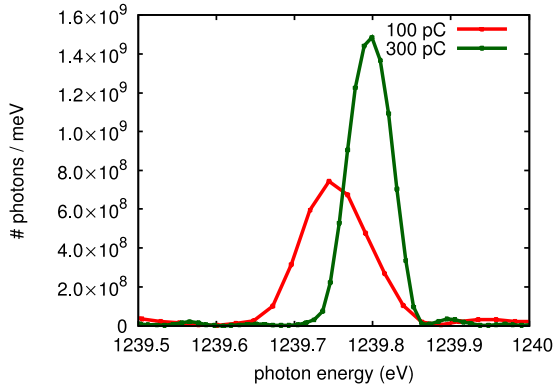

Figure 7: Output spectrum at 1 nm after 80 m.

The final x-ray pulses have a duration which is a large fraction of the electron bunch length. In fact, using flat-top seed lasers which cover the entire bunch only increase the pulse energy and duration by a modest amount.

4.1 Shorter Output Pulses

Here we examine some of the challenges with making shorter pulses. Input laser durations less than about 25 fs tend to require much more peak power both because of slippage within

the modulating undulator, and because the bunching profile can be sufficient short that slippage becomes an important effect in the radiating undulators as well. Also, the increased energy spread in the seeding region can slow down the growth rate, and allow SASE radiation in other parts of the bunch to become a significant component of the output pulse.

In Fig. 8, the power and spectrum are shown for a variety of laser profiles. When both input lasers have a duration of 200 fs fwhm, a long pulse is generated and there is hardly any SASE. When the same configuration is used but both input lasers have a duration of 100 fs fwhm, significant SASE radiation is produced in the high current region towards the tail of the bunch. In the spectrum this appears as a series of spikes at photon energies within the FEL bandwidth but separated from the seeded pulse. Because the output pulse duration is much more constrained by the duration of the second seed laser than the first, if the duration of the first and second lasers are set to 200 fs and 100 fs, respectively, the main part of the output pulse still has the same duration as when both lasers have a 100 fs duration, but the SASE background is significantly suppressed. Because the first laser also has a low peak power of 47 MW, there should be little difficulty in lengthening the second laser further to yield more suppression. On the other hand, this does add the complication that the two laser inputs cannot be generated by splitting a single pulse. As a final example, in addition to increasing the duration of the first seed laser, its peak power can be increased as well. This further suppresses SASE but at the expense of reducing the total pulse energy by roughly a factor of 2 because of the increase in energy spread in the core of the electron bunch.

Up to a point, shorter output pulses down to roughly 10 fs fwhm can be achieved, but some effort will have to be taken to suppress SASE from the head and tail of the bunch. Even 5 fs is possible if the peak power is increased to well above 1 GW – note that because of the shorter pulse duration, the actual input pulse energy required should not significantly increase.

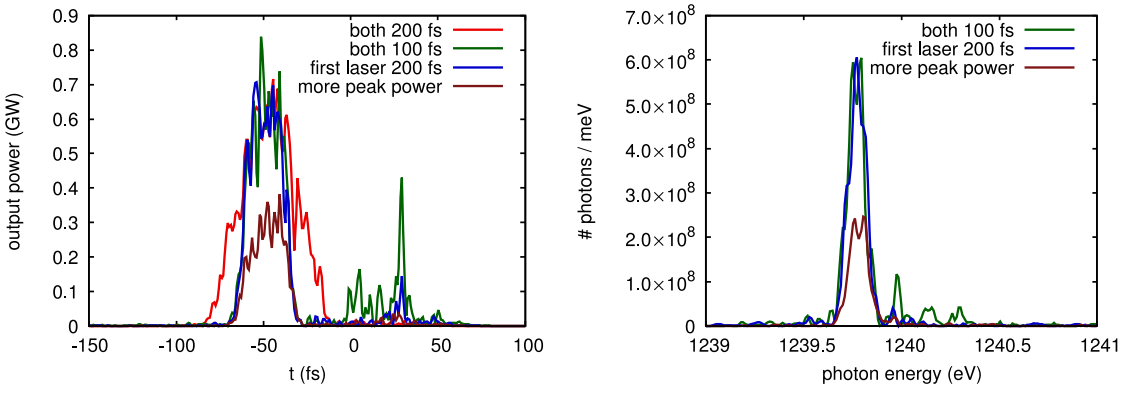

Figure 8: Output power and spectrum at 1 nm for various seed laser configurations.

4.2 Sensitivity to energy spread

Although the initial bunching is sensitive to the energy spread, as long as it is not much larger than 1 MeV the final output power should not be very sensitive to the slice energy spread. Additional undulator may be required to reach saturation, however. As an example, we consider increasing the energy spread (and energy offests) of the 100 pC bunch by a factor of 2, to almost 1 MeV in the core of the bunch. The growth of the energy in the output pulse is shown in Fig. 9. The power and spectrum are shown at both 80 m (where previous examples stopped) and at 90 m. There is a moderate reduction in pulse energy and peak spectral brightness at 80 m, which can be eliminated by adding two more undulator sections.

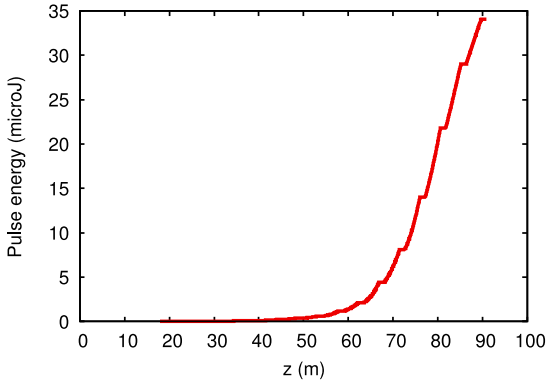

Figure 9: Evolution of pulse energy at 1 nm for the 100 pC bunch with energy spread and offsets doubled.

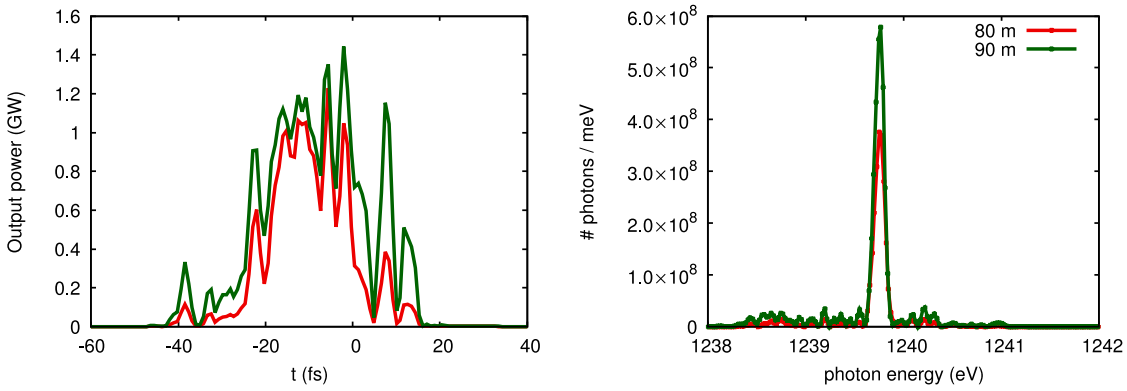

Figure 10: Output power and spectrum at 1 nm for the 100 pC bunch with energy spread and offsets doubled.

4.3 Indirect seeding to 1 nm

We now consider setting up the EEHG portion of the beamline to produce bunching at 2 nm. The peak power of the second input laser is reduced to 400 MW. We again focus on

the 100 pC bunch. The EEHG stage is then followed by 3 undulator sections tuned to 2 nm wavelength. An additional 3 sections tuned to 2 nm are required to reach saturation. If instead, the remaining undulators are tuned to 1 nm wavelength, 11 undulator sections are required to reach saturation, yielding a total pulse energy at 1 nm of 70 μJ. The increase in pulse energy compared to the nominal case for the same 80 m of beamline is due to the fact that the peak energy spread after the two modulations is reduced from 2.4 MeV to 1.8 MeV. Results are shown in Figs. 11 through 12. Note that although the power profile when the radiation at 2 nm is taken to saturation has some extra contributions from behind where the input seed lasers intersect the bunch, the spectrum is still exceptionally pure.

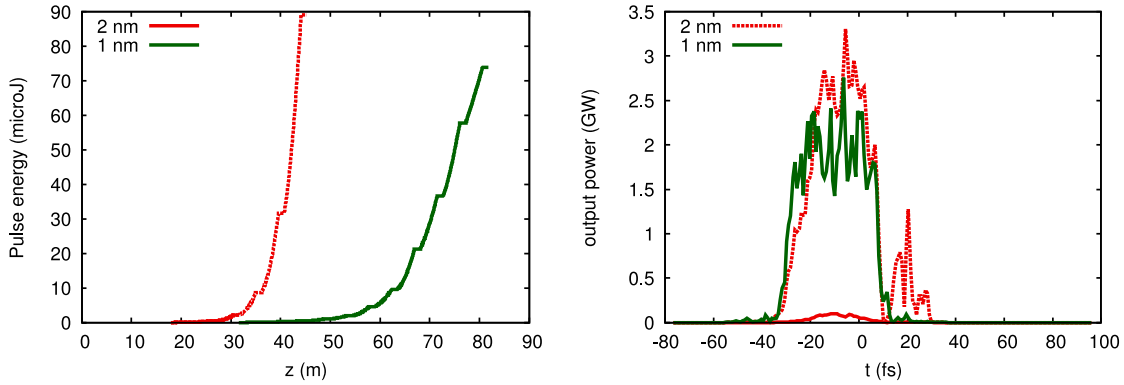

Figure 11: Pulse properties at 1 nm and 2 nm (either up to switch to 1 nm or all the way to saturation) for the 100 pC bunch with reduced EEHG harmonic. Shows the evolution of the pulse energy (left) and snapshots of the power profiles (right).

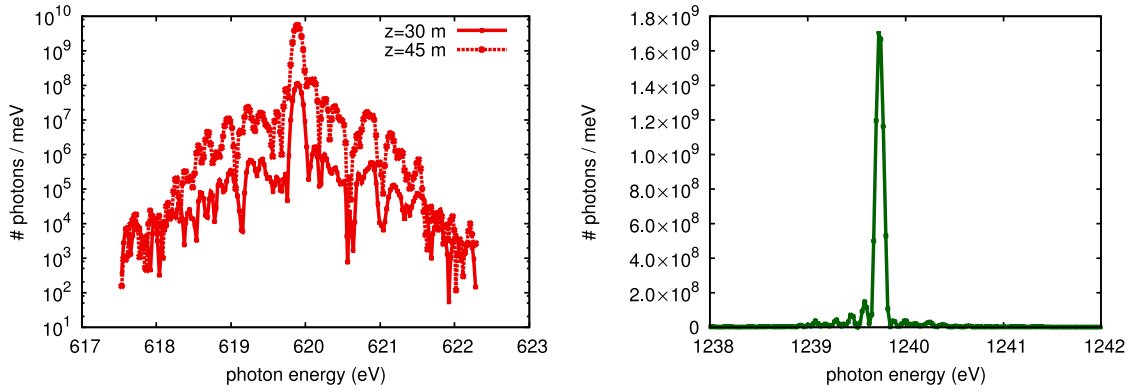

Figure 12: Output spectrum at 2 nm and 1 nm for the 100 pC bunch with reduced EEHG harmonic.

5 Conclusions

The EEHG seeding scheme should produce long pulses with good coherence, assuming that the second seed laser can be tightly controlled. In particular, sensitivity to phase noise in the input laser is a concern. The EEHG stage could produce radiation down to 1 nm either directly, or by producing bunching at 2 or 3 nm and then switching to 1 nm and radiating off of nonlinearly generated harmonic bunching. Going to even shorter wavelengths will be quite challenging, because the required energy spread induced in the beam to overcome energy scatter through IBS and ISR becomes comparable to the FEL bandwidth. Although such large harmonics will be challenging to produce, bunching at the 15th harmonic has already been demonstrated and it is hoped that further progress will be made in the near future. The EEHG scheme exhibits robustness in the face of variations in the beam parameters and beam quality, and primarily relies on a high quality, high power input laser.

References

[1] R. Bonifacio, L. De Salvo, P. Pierini, N. Piovella, and C. Pellegrini. Spectrum, temporal structure, and fluctuations in a high-gain free-electron laser starting from noise. *Phys. Rev. Lett.*, 73:70–73, 1994.

[2] J. Feldhaus, E.L. Saldin, J.R. Schneider, E.A. Schmeidmiller, and M.V. Yurkov. Possible application of x-ray optical elements for reducing the spectral bandwidth of an x-ray SASE FEL. *Optics Commun.*, 140:341–352, 1997.

[3] G. Geloni, V. Kocharyan, and E. Saldin. A novel self-seeding scheme for hard x-ray FELs. *Journal of Modern Optics*, 58:1391–1403, 2011.

[4] LCLS-II Design Study Group. 2014 LCLS-II conceptual design report. Report LCLSII-1.1-DR-0001-R0, SLAC, January 2014.

[5] G. Stupakov. Using the beam-echo effect for generation of short-wavelength radiation. *Phys. Rev. Lett.*, 102:074801, 2009.

[6] I. Ben-Zvi, K.M. Yang, and L.H. Yu. The "fresh-bunch" technique in fels. *Nucl. Instr. Meth. A*, 318:726–729, 1992.

[7] E. Hemsing, M. Dunning, C. Hast, T.O. Raubenheimer, S. Weathersby, and D. Xiang. Highly coherent vacuum ultraviolet radiation at the 15th harmonic with echo-enabled harmonic generation technique. *Phys. Rev. ST Accel. Beams*, 17:070702, 2014.

[8] S. Reiche. GENESIS 1.3: a fully 3D time-dependent FEL simulation code. *Nucl. Instr. Meth. A*, 429:243–248, 1999.

[9] G. Penn. Intra-beam scattering for free electron lasers and its modeling in chicanes. LBNL Report LBNL-6762E, LBNL, August 2014.

[10] R. Bonifacio, L. De Salvo Souza, and P. Pierini. Generation of XUV light by resonant frequency tripling in a two-wiggler FEL amplifier. *Nucl. Instr. Meth. A*, 296:787–790, 1990.